

A SIMPLE MODEL OF THE ATMOSPHERIC BOUNDARY LAYER; SENSITIVITY TO SURFACE EVAPORATION

IB TROEN

Risø National Laboratory, 4000 Roskilde, Denmark

and

L. MAHRT

Department of Atmospheric Sciences, Oregon State University, Corvallis, OR 97331, U.S.A.

(Received in final form 30 April, 1986)

Abstract. A simple formulation of the boundary layer is developed for use in large-scale models and other situations where simplicity is required. The formulation is suited for use in models where some resolution is possible within the boundary layer, but where the resolution is insufficient for resolving the detailed boundary-layer structure and overlying capping inversion. Surface fluxes are represented in terms of similarity theory while turbulent diffusivities above the surface layer are formulated in terms of bulk similarity considerations and matching conditions at the top of the surface layer. The boundary-layer depth is expressed in terms of a bulk Richardson number which is modified to include the influence of thermals. Attention is devoted to the interrelationship between predicted boundary-layer growth, the turbulent diffusivity profile, 'countergradient' heat flux and truncation errors.

The model predicts growth of the convectively mixed layer reasonably well and is well-behaved in cases of weak surface heat flux and transitions between stable and unstable cases. The evolution of the modelled boundary layer is studied for different ratios of surface evaporation to potential evaporation. Typical variations of surface evaporation result in a much greater variation in boundary-layer depth than that caused by the choice of the boundary-layer depth formulation.

1. Introduction

The present study develops a relatively simple model of the atmospheric boundary layer for applications where high vertical resolution is not possible. For example, the present development is partly motivated by the need to study interactions between the atmospheric boundary layer and soil moisture transport which is examined in a companion paper (Pan and Mahrt, 1986). Because the formulation of the surface evaporation is necessarily crude, a high-resolution sophisticated model of the boundary layer is not justified for such applications.

In this study, considerable attention will be devoted to development of a boundary-layer depth formulation which: (1), does not require resolution of the capping inversion, when it exists; (2), allows for a continuous transition between the stable and unstable boundary layer; (3), describes the near-neutral case where the surface heat flux is unimportant; and (4), removes certain inconsistencies between the application of surface similarity theory and the 'countergradient' flux correction.

A number of boundary-layer models with low resolution have been proposed for use in large-scale models. One approach is to model the bulk effect of the boundary layer by interpolating pertinent variables from the large-scale model without attempting to resolve any boundary-layer structure explicitly (e.g., Clarke, 1970; Deardorff, 1972; Smeda, 1979; Chang, 1981; Binkowski, 1983).

In models where some grid levels are available to resolve boundary-layer structure, a more direct approach is usually adopted by expressing turbulent diffusivities in terms of local gradients of the mean profiles. Models of this kind have been used mostly in cases where comparatively high resolution is available (column models); then diffusivities are related directly to the local gradient Richardson number (Zhang and Anthes, 1982), or to a Richardson number adjustment scheme (Chang, 1979), or computed in conjunction with a prescribed mixing-length profile (Busch *et al.*, 1976; Louis, 1979). With coarser resolution, the sensitivity of these formulations to small changes in the mean profiles becomes a disadvantage. Inclusion of transport terms by employing the turbulence energy equation (e.g., Mailhôt and Benoit, 1982; Therry and Lacarrère, 1983) or even higher order closure schemes (e.g., Yamada and Mellor, 1975; André *et al.*, 1978) is presently not practical for use in large-scale models because of the large computational requirements.

Here we develop a model, where turbulent diffusivities have a prescribed profile shape as a function of z/h and scale parameters derived from similarity arguments, where z is the height above ground and h is the boundary-layer top. This approach partially alleviates resolution requirements and is yet more flexible than the purely 'bulk' models.

Similar approaches for the simulation of the heated boundary layer have been applied by Pielke and Mahrer (1975), and Yu (1977). The present model, however, differs from these approaches both with respect to the profile formulations and the way the boundary-layer height is determined. The present model appears to be less specialized than the usual mixed-layer growth models but still does not consider the important problem of boundary-layer clouds.

2. The Model

2.1. THE SURFACE BOUNDARY LAYER

The surface-layer parameterization scheme devised by Louis (1979) is used to relate surface fluxes of heat, momentum, and water vapour to the values of temperature, the wind components and specific humidity, all at the lowest model level. The layer between the surface and the lowest model level is thus considered to be in equilibrium, obeying surface-layer similarity. The basic advantage of this formulation is computational efficiency, since the formulation avoids an iterative process which is otherwise necessary when employing the original expressions given by Businger *et al.* (1971) for the usual range of atmospheric stability; however, the correct behaviour of such formulations is uncertain in the cases of extreme stability or instability.

2.2. THE BOUNDARY LAYER ABOVE THE SURFACE LAYER

Above the surface layer, the diffusion equation is assumed to describe the effect of turbulent mixing in the boundary layer except for the modification due to a 'counter-gradient' term. Thus, model closure simplifies essentially to the determination of the diffusivity profiles.

As in Brost and Wyngaard (1978), the momentum diffusivity is modelled according to the format

$$K_m = u_* k z \Phi_m^{-1} \left(1 - \frac{z}{h} \right)^p, \quad (1)$$

where u_* is the surface friction velocity, k is the von Karman constant taken to be 0.40, Φ_m is the nondimensional shear, z is the height above ground, and h is boundary-layer height. Equation (1) is consistent with surface-layer similarity where

$$K_m = u_* k z \Phi_m^{-1} \quad \text{for } z \ll h. \quad (2)$$

For stable conditions we use Φ_m from Businger *et al.* (1971) given as

$$\Phi_m = 1 + 4.7z/L, \quad (3)$$

where L is the Monin-Obukhov length. For $z \gg L/4.7$, combination of Equations (1) and (3) yields the following asymptotic expression:

$$K_m \simeq (k/4.7)Lu_* \left(1 - \frac{z}{h} \right)^p. \quad (4)$$

That is, for the stable case L becomes the relevant length scale and u_* the relevant velocity scale for the entire boundary layer. Here the boundary-layer depth h enters only as the height at which the turbulence vanishes and does not influence the boundary-layer velocity scale.

For unstable conditions

$$\Phi_m(z/L) = (1 - 7z/L)^{-1/3}, \quad z \ll h. \quad (5)$$

The exponent of $-1/3$ is chosen to ensure the free-convection limit for $z \gg L$. With the coefficient chosen to be 7, the difference between Equation (5) and the original expression given by Businger *et al.* (1971) as derived from the Kansas data differs by less than 6% over the range of the original data ($-z/L < 2$). Here we consider the surface layer to extend upward to $z = \varepsilon h$ where ε will be arbitrarily specified to be 0.1.

Above the surface layer for the unstable case, we arbitrarily assume that the relevant velocity scale $u_* \Phi_m^{-1}$ is constant so that using (5)

$$u_* \Phi_m^{-1} = (u_*^3 + 7\varepsilon k w_*^3)^{1/3} \equiv w_s, \quad (6)$$

where Φ_m is evaluated at εh and $w_* = (g/T_0) \overline{w' \theta'_0 h}^{1/3}$ is the convective velocity scale.

Then (1) becomes

$$K_m = w_s h k \frac{z}{h} \left(1 - \frac{z}{h}\right)^p, \quad z > \varepsilon h. \quad (7)$$

For $h \gg -L$, the velocity scale approaches

$$w_s \simeq w_* (7\varepsilon k)^{1/3} \simeq 0.65 w_* . \quad (8)$$

Note that the transition between stable and unstable cases is continuous.

The expression for the mixed-layer velocity scale (6) can be compared with the velocity scale developed by Hojstrup (1982) from the Kansas and Minnesota experiments. Hojstrup's expressions for the velocity variances at $z/h = \varepsilon = 0.1$, reduce to

$$w_s = (\sigma_u^2 + \sigma_v^2 + \sigma_w^2)^{1/2} = 2.26 u_* \left(1 + 2.75 \left(0.1 \frac{h}{-L}\right)^{2/3}\right)^{1/2}. \quad (9)$$

Apart from a constant factor of proportionality, Equations (6) and (9) differ by less than 16% in the range of $h/-L$ between 0 and 5000, in which range w_s changes by a factor of 13.

With the factor $(1 - z/h)^p$ in (7), the turbulent mixing approaches zero at the top of the boundary layer. This condition should be relaxed in models which allow mixing above the boundary-layer top.

3. Determination of Boundary-Layer Depth

For well-defined diurnal variations, a rate equation for growth of the daytime mixed layer is often used with a separate model for the depth of the nocturnal boundary layer. The transition from unstable to stable conditions then requires special consideration (Smeda, 1979). With modest increase of complexity, it is possible to unify the depth prediction into one relationship (Binkowski, 1983). These models successfully predict the diurnal variation of the boundary layer under conditions of significant diurnal signature.

With weak surface heating and complex synoptic airflow, the top of the daytime boundary layer and capping inversion are often not well-defined and the usual mixed-layer growth equations become too specialized. Even in situations with definable mixed-layer growth, the vertical resolution in many atmospheric models is inadequate to define the capping inversion and corresponding velocity jump required for mixed-layer growth models (e.g., Manins, 1982).

Alternatively, Busch *et al.* (1976) chose the boundary-layer top to be the lowest model layer where the gradient Richardson number exceeds a critical value. This method, however, still requires good resolution, and even with high resolution may lead to large unphysical oscillations of h due to the sensitivity of the gradient Richardson number to small changes in the mean profiles.

To be consistent with the bulk approach adopted in Section 2, we determine the boundary-layer top by specifying the value of a modified Richardson number such that

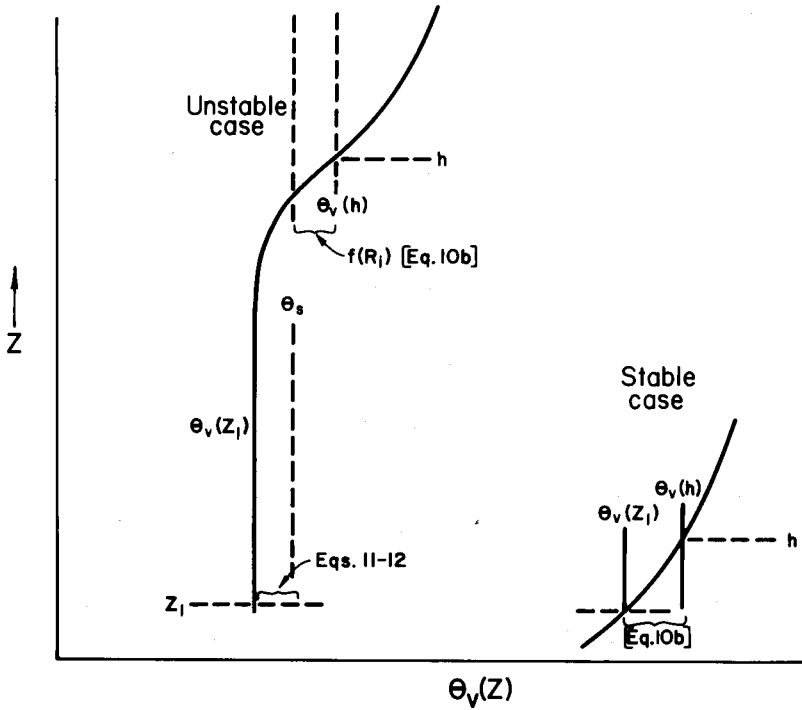


Fig. 1. Geometric sketch of the boundary-layer depth relationship to the profile of potential temperature above the surface layer (solid profile). For the unstable case, the first vertical broken line to the right of the profile indicates the potential temperature after enhancement due to the temperature excess associated with surface heating (11-12). The vertical broken line on the right indicates the potential temperature at the boundary-layer top after deepening due to shear-generated mixing as formulated in terms of a modified bulk Richardson number (10b). The latter mechanism completely determines the depth of the stable boundary layer.

$$h = \text{Ri} \frac{T_0 |\mathbf{v}(h)|^2}{g(\theta_v(h) - \theta_s)}, \tag{10a}$$

where $\theta_v(h)$ is the virtual potential temperature at the boundary-layer top and θ_s is defined below (Figure 1). The bulk Richardson number is frequently used to model the depth of the stable boundary layer where θ_s is chosen to be the temperature of the air near the surface. By relating θ_s to the temperature of thermals via the usual 'counter-gradient' heat flux correction for the unstable case, it will be shown that relationship (10a) also approximates the growth of the daytime mixed layer as well as allows treatment of cases with weak surface heat flux and transitions between stable and unstable cases.

At each time step, the model incrementally increases the test value of h until $\theta_v(h)$ and the corresponding modified bulk Richardson number have increased to yield the specified critical value of the modified bulk Richardson number. In the heated boundary

layer, the boundary-layer top predicted by (10a) occurs just above the well-mixed region since $\theta_v(h)$ is greater than θ_s for nonzero wind speed and θ_s is larger than the mixed-layer temperature for nonzero surface heat flux. This is evident by writing (10a) in the form

$$\theta_v(h) = \theta_s + \text{Ri}_c |\mathbf{v}(h)|^2 / (hg/\theta_0). \quad (10b)$$

This relationship shows that the thickness of the implied entrainment region, between the well-mixed region and predicted boundary-layer top, depends on the definition of the near-surface air temperature, on the wind speed, and indirectly on free-flow stratification (Figure 1). For significant surface heating, the second term exerts only a minor influence on boundary-layer depth which then becomes insensitive to the value of the Richardson number.

In the case of vanishing wind speed, and thus vanishing shear generation of turbulence, relationship (10a) becomes analogous to the thermodynamic approaches applied in Holzworth (1964) and Zhang and Anthes (1982). In this model, (10a) reduces to the asymptotic prediction for free convection

$$\theta_v(h) = \theta_s.$$

The choice of the near-surface atmospheric temperature θ_s in (10a) plays an important role. Since the most energetic transporting scales of turbulent motion in the convective boundary layer are thermals, it seems more correct to define θ_s as a measure of temperature of the thermals in the lowest part of the boundary layer as in Zhang and Anthes (1982). This can be estimated from the relevant velocity scale w_s corresponding to a thermal turnover time of h/w_s . The scaled virtual temperature excess near the surface is then

$$\theta_T = C \frac{\overline{(w' \theta'_v)_0}}{w_s} \quad (11)$$

where $\overline{(w' \theta'_v)_0}$ is the surface virtual kinematic heat flux and C is a coefficient of proportionality. Use of this temperature excess to estimate the boundary-layer top from (10a) could be viewed as a parcel approximation which neglects the influence of entrainment and pressure effects on the thermal ascent. This overestimation of thermal ascent would be partially compensated by neglect of penetration of thermals beyond the buoyancy equilibrium level. The attempt to include such complexities in a limited resolution model would not be appropriate due to large truncation errors. Relationship (11) is consistent with the heat flux correction as discussed in Section 4.

For simplicity, the temperature excess (11) is assumed to occur at the lowest atmospheric level in the model, z_1 . Then

$$\theta_s = \theta_v(z_1) + \theta_T. \quad (12)$$

For the unstable case, the modelled boundary-layer depth (10–12) depends mainly on the temperature excess and is insensitive to the choice of the critical Richardson number. An equivalent prognostic relationship between boundary-layer growth rate and surface

heat flux can be derived by differentiating (10), after using (11–12). It will be found that use of (10) with (11–12) predicts the growth of the heated mixed layer with success comparable to the use of the growth relationship of Deardorff (1974). That is, for the sole purpose of approximating the boundary-layer growth rate, the approximate role of the convective heating can be captured rather simply. Naturally in high resolution studies of the boundary layer, the more complete physics of mixed-layer growth models would be desirable.

As we approach neutral conditions from the unstable side, θ_T in (11) vanishes. Relationships (11) and (12) are not relevant for the stable boundary layer. Since the first model level may be above the nocturnal boundary layer, θ_s is defined to be the surface virtual temperature for the stable case. In low-resolution large-scale models, the structure of the nocturnal boundary layer cannot be resolved so that only bulk formulations can be implemented. The use of the bulk Richardson number (10) to predict the top of the nocturnal boundary layer has been tested in a number of studies (some of which are surveyed in Mahrt, 1981), and provides a smooth transition to the unstable case in the present model.

In such studies the critical bulk Richardson number is typically chosen between 0.3 and 1. Such values are sometimes tested against the depth of the nocturnal inversion which may be considerably thicker than the depth of the layer of continuous turbulence (Mahrt *et al.*, 1979; André and Mahrt, 1982). On the other hand, we must recognize that model fluxes imply both time and horizontal averaging. Such averaging would then include transport induced by meso-scale and terrain-induced circulations which seem to be important in the nocturnal boundary layer even over very weak slopes. Furthermore, fluxes may occur locally in space and time even though the Richardson number evaluated from averaged variables is large. These factors suggest choosing a larger critical Richardson number for computing the boundary-layer depth in large-scale models. Here we chose a value of one-half for use in one-dimensional simulations.

In the stable case, the modelled boundary-layer depth exerts less influence on the strength of the mixing as is evident by comparing (4) and (7). That is, the implied length scale of the mixing asymptotically becomes independent of h and proportional to L . In the unstable case, the value of h significantly influences the length scale above the surface layer; however, the value of h becomes insensitive to the bulk Richardson number.

4. The Diffusivities for Heat and Water Vapour

We make the usual assumption of equating diffusivities for heat and water vapour. The turbulence Prandtl number $Pr = K_h/K_m$ under unstable conditions is found to be strongly dependent on stability in the surface layer (Businger *et al.*, 1971). In the mixed layer above the surface layer, the Prandtl number is not very well-defined because local gradients may vanish and fluxes become more related to bulk gradients. Thermals and eddies of boundary-layer scale transport heat and other properties according to bulk gradients which may be much larger than, or of opposite sign from, gradients in the boundary-layer interior.

The simplest way to include this nonlocality is to incorporate a 'countergradient' term as discussed by Priestley and Swinbank (1947) and Deardorff (1966). Then the heat flux becomes

$$\overline{w' \theta'} = -K_h \left(\frac{\partial \theta}{\partial z} - \gamma \right). \quad (13)$$

In the present formulation

$$\gamma = C \frac{(\overline{w' \theta'})_0}{w_s h}. \quad (14)$$

This prescription is consistent with the formulation of the temperature excess for thermals, (11). A similar correction procedure was suggested by Deardorff (1973) and used in the model by Mailhôt and Benoit (1982), except that the free-convection velocity scale w_* was chosen to be the velocity scale. The use of the velocity scale w_s (9) is more consistent with the formulation of the eddy exchange coefficient and includes the reduction of thermal buoyancy by mechanical mixing.

This interrelationship is clearest at the level where the potential temperature gradient vanishes as it reverses with height from weakly unstable to weakly stable. At this level, say $z = z^*$, Equation (13) becomes

$$(\overline{w' \theta'})_{z^*} = K_h(z^*) \gamma$$

or using (14)

$$C = \frac{h w_s}{K_h(z^*)} \frac{(\overline{w' \theta'})_{z^*}}{(\overline{w' \theta'})_0}.$$

This relationship exemplifies the fact that C cannot be specified independently of the formulation of K_h as has been done in previous studies and also shows how the coefficient C controls the level of vanishing temperature gradient. Substituting in the formulation for K_h , the expression for C becomes

$$C = \left[\text{Pr } k \frac{z^*}{h} (1 - z^*/h)^p \right]^{-1} \left[\frac{(\overline{w' \theta'})_{z^*}}{(\overline{w' \theta'})_0} \right].$$

Choosing, for example, $p = 2$, $\text{Pr} = 2$, $z^*/h = 1/2$ and $1/2$ for the heat flux ratio, one obtains the value of $C \approx 5$. Since the results in this study were found to be not sensitive to the numerical value of C , we adopt the usual value of 10 for C' (see Equation (19) below), corresponding to $C = 6.5$.

It seems necessary to adopt a countergradient correction term for transport of moisture or any scalar, since thermals also transport according to the bulk moisture gradient and therefore create flux, even where the local mean gradient vanishes. We then define the countergradient factor for moisture by assuming that it can be formulated with the same coefficient C as for heat transport in which case

$$\gamma_q = C \frac{(\overline{w'q'})_0}{hw_s}, \quad (15)$$

where $(\overline{w'q'})_0$ is the surface moisture flux. An analogous correction for momentum is not adopted. Because of the pressure effects, thermals cannot efficiently transport momentum over large distances and the gradient of momentum often remains significant throughout the mixed layer.

4.1. PRANDTL NUMBER

Busch *et al.* (1976) assume that the Prandtl number obeys surface-layer relations for the entire boundary layer while Mailhôt and Benoit (1982) assume that the Prandtl is independent of height with a value computed at 4 m. In the present development, we match heat and momentum fluxes at the top of the surface layer so that

$$u_* \theta_* = K_h \left(\frac{\partial \theta}{\partial z} - \gamma \right), \quad u_*^2 = K_m \frac{\partial u}{\partial z}, \quad (16)$$

where $\theta_* \equiv -(\overline{w'\theta'})_0/u_*$. Combining these two relationships, using the usual definitions of nondimensional gradients (Φ_m, Φ_h) and the definition of w_s (6), substituting for γ from (14) and solving for the Prandtl number, we obtain

$$\text{Pr} = \frac{K_h}{K_m} = \left[\frac{\Phi_h}{\Phi_m} \left(\frac{z}{L} \right) + k \frac{z}{h} C \right]^{-1}, \quad (17)$$

where z is the level where matching (16) is applied, here taken as $0.1h$. Lacking other evidence, we assume that the Prandtl number is independent of height above $0.1h$. The Prandtl number is bounded by the asymptotic limits of unity and four. Expression (17) has the advantage that it is well behaved for vanishing Monin–Obukhov length L .

4.2. COMPARISON WITH WYNGAARD AND BROST

It is instructive to compare the diffusivity profile used here with the one derived from the large eddy simulations by Wyngaard and Brost (1984). They derive expressions for the gradients of a scalar for the case of vanishing entrainment flux (their Equation (33)) and for the case of vanishing surface flux (their Equation (39)). Profile functions were determined by comparing with numerical simulations for the case $-z/L = 64$. When both fluxes are present, we can obtain the effective diffusivity from their individual relationships. Assuming the flux in the boundary layer to vary linearly with height, the diffusivity relationship derived from Wyngaard and Brost (1984) becomes

$$K = w_* h \frac{\left(1 - (1 - R) \frac{z}{h} \right)}{R \left(1 - \frac{z}{h} \right)^{-3/2} + 0.4 \left(\frac{z}{h} \right)^{-3/2}}, \quad (18)$$

where $R = (\overline{w'c'})_h/(\overline{w'c'})_0$ and c is the transported quantity.

As discussed by Wyngaard and Brost (1984), this form is not well-behaved since the transport by large eddies or thermals is not directly related to the local gradients. The simplest way to include this transport process effectively is again to adopt a gradient correction factor γ such that

$$\overline{w'c'} = -K \left(\frac{\partial \bar{c}}{\partial z} - \gamma_c \right), \quad \gamma \equiv C' \frac{(w'c')_0}{w_* h}, \quad (19)$$

where the prime notation on the coefficient C' indicates that the free-convection velocity scale w_* must be used instead of w_s in order to be consistent with (18). Then using the gradient and flux from Wyngaard and Brost (1984), the diffusivity satisfying (19) and the gradient correction γ (14), becomes

$$K = w_* h \frac{\left(1 - (1 - R) \frac{z}{h} \right)}{R \left(1 - \frac{z}{h} \right)^{-3/2} + 0.4 \left(\frac{z}{h} \right)^{-3/2} + C'} \quad (20)$$

The diffusivity profile modified to include the countergradient correction (20) is shown in Figure 2 for different values of R , the ratio of the entrainment flux to the surface flux.

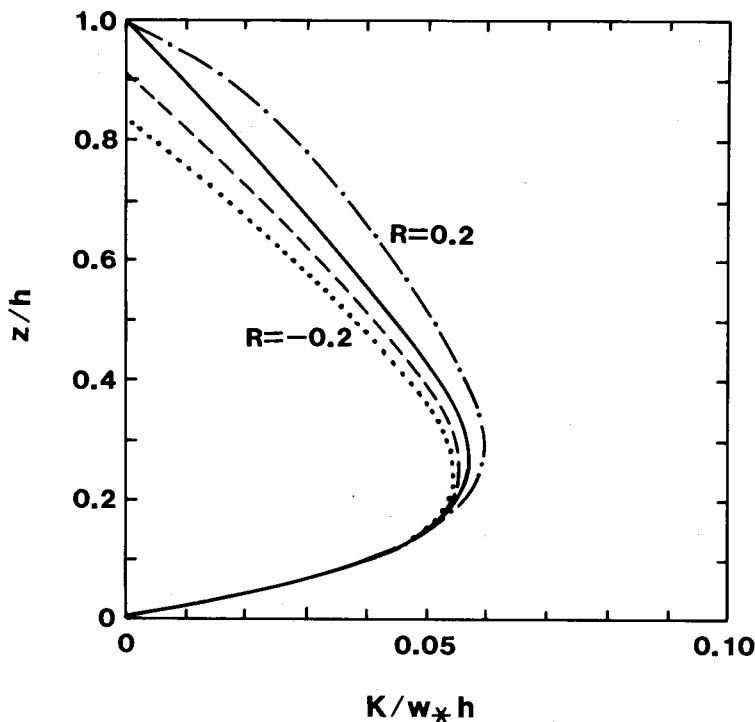


Fig. 2. The profile of diffusivity from Equation (20) for different values of R , the ratio of entrainment flux to the surface flux. $R = 0.2, -0.1, 0.0$, and 0.2 .

C' has been assigned the value of 10 as in previous studies. Equation (20) and Figure 2 indicate that with the addition of the countergradient correction, the diffusivity profile is well behaved and only moderately sensitive to the value of the ratio R except for a thin layer near the boundary-layer top where the diffusivity oscillates for $R < 0$ (not resolved in Figure 2).

4.3. THE EXPONENT p

In the case of the diffusivity for heat, the ratio R is often approximated as -0.2 (Tennekes, 1973). The profile for the heat diffusivity based on (17) for values of the exponent p between 2 and 3, agrees with the corresponding profile in Wyngaard and Brost (1984) for $R = -0.2$ except that the heat diffusivity is somewhat larger in the middle of the boundary layer (Figure 3). Comparison with Wyngaard and Brost for heat diffusivity is not entirely correct for values of R other than those appearing in their model because of the dynamical influence of the heat flux. For the results cited here they found $R = -0.1$.

Near the top of the boundary layer, behavior of the diffusivity determines the importance of the entrainment flux. The diffusivity appears to vanish; however, the computed heat flux in low-resolution models remains significant depending mainly on

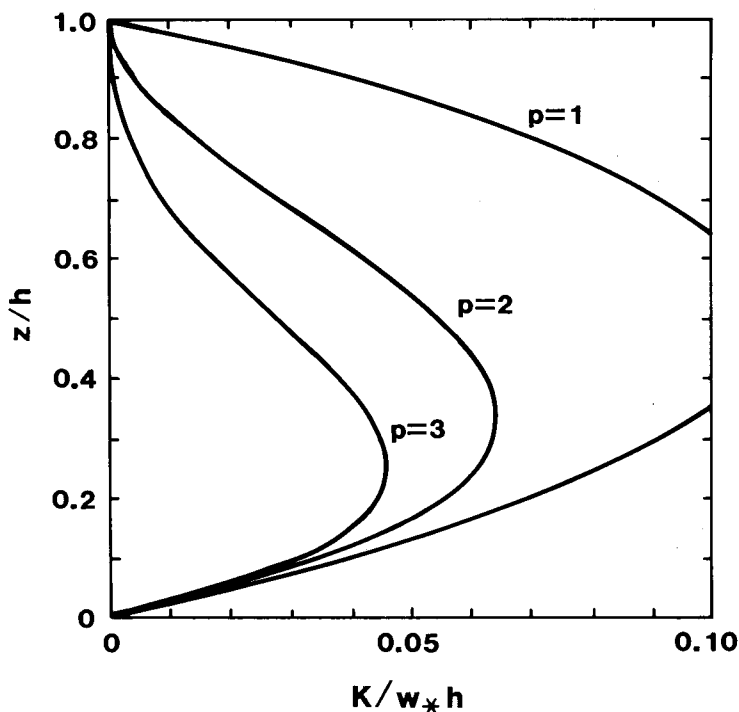


Fig. 3. The profile of diffusivity for heat and water vapour in the present model in the case of a heated boundary layer with parameters taken from Wyngaard and Brost (1984). Numbers on the graphs give the values of p in Equation (1).

the way in which the boundary-layer height is determined and on truncation errors. This problem is analogous to the difficulty where mixed-layer growth predictions are sensitive to the way in which the 'jumps' are estimated at the mixed-layer top (Anthes *et al.*, 1982). Since the entrainment zone cannot be resolved, we use the exponent p as an adjustable parameter chosen to give reasonable values for the flux ratio R in a particular model with a particular resolution. It is obvious that the exponent p could be dependent on stability. For example, Brost and Wyngaard (1978) choose 1.5 for the stable case. For simplicity, and lack of observational evidence, we presently specify p to be independent of stability with a constant value of 2.

4.4. RESOLUTION

For the numerical iterations of this study, a vertical resolution of 50 m is used since computer time is not a significant factor in the one-dimensional model. As the resolution is sequentially decreased to 500 m for a vertical domain of 2 km, the difference between the boundary-layer depth of the high-resolution and the low-resolution models is always less than the vertical grid spacing of the low-resolution model. As the resolution is decreased to less than 500 m, the predicted time-evolution of the model begins to rapidly degenerate. When used in concert with a general circulation model, we have used five levels between the surface and 2 km with reasonable results for a variety of synoptic situations.

5. Boundary-Layer Depth Prediction

Boundary-layer models operating within larger scale models must not only approximate the commonly studied convectively mixed layer but also must approximate cases where surface heating is weak and the mean wind is strong. Here we examine the response of the boundary layer to different values of the geostrophic wind speed and incoming solar radiation. We concentrate on the model performance of the boundary-layer depth which represents the most important deviation from previous modelling. Results are now compared with the frequently used boundary-layer depth formulation of Deardorff (1974), which is the primary existing depth model which does not require resolution of the capping inversion.

Figure 4 displays the sensitivity of these two formulations to variations of the specified incoming solar radiation and geostrophic wind speed for an initial vertical gradient of potential temperature of 6 C km^{-1} and zero surface evaporation and zero heat exchange with the subsurface. The depth of the model domain is 4 km. The downward longwave radiation is constant at 330 W m^{-2} . The specified downward shortwave radiation varies diurnally according to the zenith angle arbitrarily chosen to be that of the Wangara field program. The abscissa in Figure 4 represents the noontime maximum value scaled by the value for Wangara Day 33 (470 W m^{-2}). As the noontime downward solar radiation becomes small, the boundary layer remains stable the entire day.

For significant surface radiative heating, the two approaches lead to almost identical predictions within the vertical resolution of 50 m (Figure 4). However, with weak surface

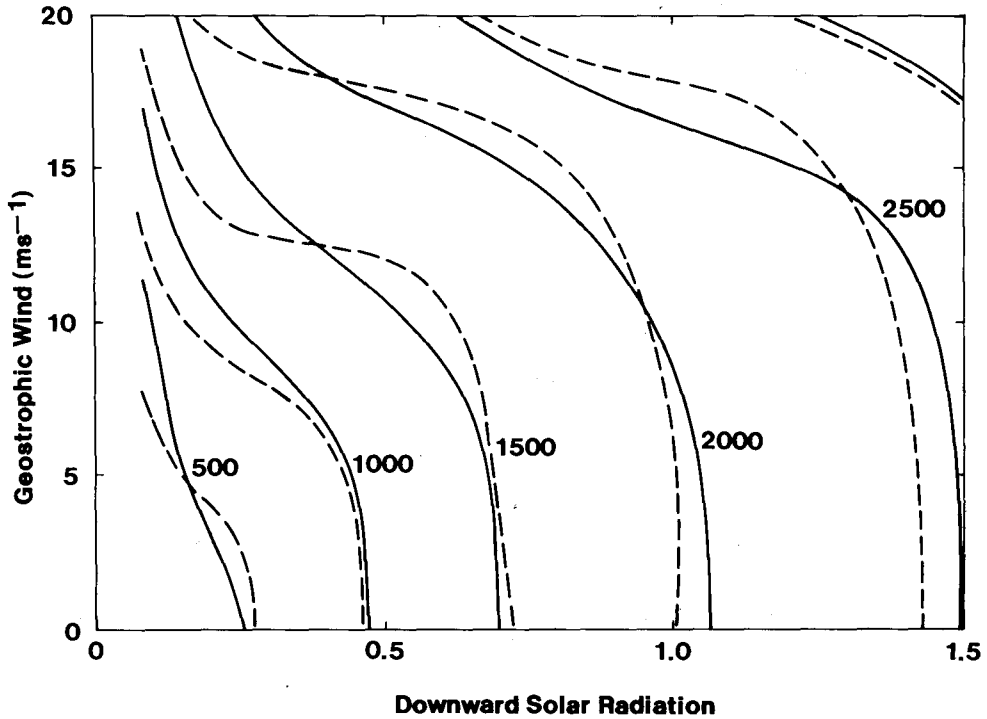


Fig. 4. Isolines of maximum boundary-layer depth for the present model (solid lines) and the Deardorff depth formulation (broken lines) as a function of geostrophic wind and scaled noontime downward solar radiation (see text).

heat flux and strong winds, the present formulation predicts boundary-layer depths which are significantly less than those obtained using Deardorff's model. For these cases, comparisons between the two models depend significantly on the specified Richardson number of the present model, the Coriolis parameter (here the Wangara value) and the way in which the free-flow stratification is computed for the Deardorff formulation. Judgements cannot be made because of limited observational evidence for such conditions and the difficulties of assessing the role of advection, vertical motions, and surface evaporation.

However, it is possible to delineate physical differences for the case of vanishing surface heat flux. The boundary-layer depth of the Deardorff model approaches $\frac{1}{3}u_* / f$ at a rate which is inversely proportional to the free-flow stratification. In the present formulation, the boundary-layer depth with negligible surface heating approaches $\frac{1}{2}u^2 / (g(\Delta\theta/\theta_0))$, where $\Delta\theta$ is again the temperature difference across the boundary layer. The first formulation would appear to lead to large depths at low latitudes, although any subsidence or advection, even if weak, helps limit the modelled boundary-layer growth. In the second formulation, Coriolis influences are only indirect through control of the wind field. The role of the Earth's rotation on the boundary-layer depth remains an

unresolved issue, since this influence on the observed boundary-layer growth cannot be separated from constraints of stratification and subsidence. In theoretical periodic flows, the Earth's rotation may even increase the boundary-layer depth (e.g., Holton *et al.*, 1971). Such near-neutral boundary layers occur often when attempting to model the atmosphere on a day-to-day basis. However, such cases are rarely studied rigorously from a boundary-layer point of view.

6. Model Comparison

In this section, we perform the usual comparison with Wangara days 33 and 34. The intention is to show that the model yields reasonable results. It will also be shown that these comparisons, as well as previous ones in the literature, are not very accurate because of uncertainties in the surface moisture flux. The importance of these uncertainties can be anticipated from the results of McCumber and Pielke (1981) and Manins (1982).

In this study, the surface evaporation E is specified to be a fixed fraction β of the potential evaporation E_p , where the latter depends only on atmospheric variables (Appendix A):

$$E = \beta E_p .$$

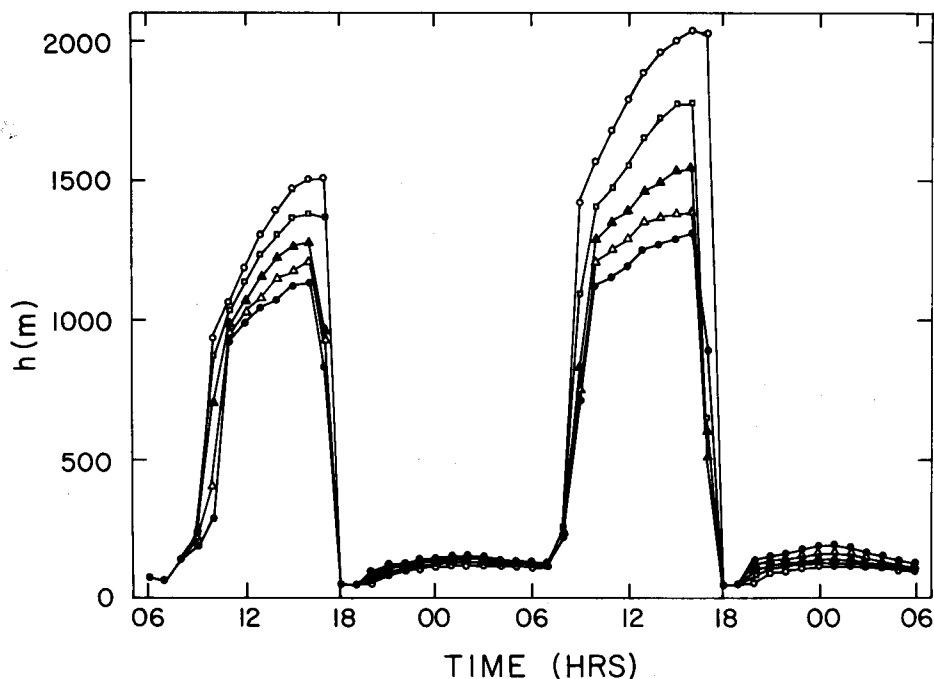


Fig. 5. The boundary-layer depth as a function of local standard time for water availability $\beta \equiv E/E_p = 0$ (open circles), 0.25 (open squares), 0.5 (solid triangles), 0.75 (open triangles), and 1 (solid circles).

The moisture availability parameter β will be varied to reveal the sensitivity of the model.

For the model runs, we specify the initial conditions to be the observed atmosphere at 0600 LST on Wangara day 33 (Clarke *et al.*, 1971). The model is integrated for a 48-hr period using the solar radiation expression of Holtslag and Van Ulden (1983) and computing the downward longwave radiation by assuming a reference temperature of 270 K at $z = \infty$.

As the specified water availability factor $\beta \equiv E/E_p$ increases from zero (no surface evaporation) to 0.25 and then 0.5, the daytime boundary-layer growth rate decreases significantly (Figure 5). Further increases of β lead to progressively smaller changes. *This nonlinear dependence of boundary-layer growth rate on water availability is due to the reduction of potential evaporation associated with increased relative humidity of the boundary layer. This negative feedback is also assisted by the reduction of surface heating due to surface evaporation, which in turn reduces the downward mixing of drier air and reduces the surface wind speed. In spite of these negative feedback mechanisms, the boundary-layer growth is quite sensitive to variations between no surface evaporation and modest surface evaporation. The differences between the present simple model of boundary-layer depth results using the depth model of Deardorff, and the observed mixed-layer depth are all smaller than the influence of usual uncertainties of the surface evaporation rate. Most of the boundary-layer growth can be predicted in terms of simple conservation of heat without concern for the details of the entrainment rate. This suggests that models need more emphasis on correct prediction of the surface heat flux, which in turn requires determination of the surface evaporation.

The evaluation of the depth of the nocturnal boundary layer is more difficult. For example, estimates in the literature disagree on the value of the 'observed depth' by more than a factor of two. The decreases of the modelled depth after midnight is due to the flow deceleration which occurs both in the model and in the observed flow. This deceleration appears to be associated primarily with the nocturnal inertial oscillation and associated variation of shear.

7. Conclusions

This study develops a numerical model of the atmospheric boundary layer which requires only modest vertical resolution and is sufficiently simple for use in concert with other models. For example, the formulation of boundary-layer depth includes the main features of mixed-layer growth but does not lead to special interpolation problems which occur with the use of more sophisticated mixed-layer growth formulations in models with low vertical resolution. The simple boundary-layer depth model adopted here includes the influences of mixing generated by both shear and surface heating and allows for a smooth transition to the stable case and well-behaved treatment of flows with weak surface heat flux. The 'countergradient correction' to the heat transport by convective eddies of boundary-layer scale has been generalized to be consistent with surface-layer similarity theory and at the same time to permit continuous transition to the mechanically mixed boundary layer.

The boundary-layer depth formulation produces results similar to those of the Deardorff (1974) formulation and the model yields results comparable to the observed depth for Wangara days 33 and 34. However, definitive tests are not possible because of uncertainties in the observed surface moisture flux. The model prediction is sensitive to such uncertainties in spite of compensating feedbacks.

Acknowledgments

We gratefully acknowledge Professor Hua-Lu Pan for extensive modelling advice and comments and the helpful detailed comments of Kenneth Mitchell and the reviewer. This work was supported by Contract No. F19628-81-K-0046 from AFGL, Cambridge MA., U.S.A.

Appendix A. Surface Energy Balance

We assume that the model input from the radiation calculations in the larger scale model includes both short- and long-wave contributions. The surface energy balance (W m^{-2}) then becomes

$$(1 - \alpha) S_{\downarrow} + L_{\downarrow} - \sigma T_0^4 = G + H + E, \quad (\text{A1})$$

where S_{\downarrow} is the downward shortwave radiation, α is the albedo, L_{\downarrow} downward long-wave radiation, G the ground heat flux, positive when downward, H and E are the sensible and latent heat fluxes, respectively, positive when upward.

The latent heating is related to the potential evaporation through the relationship

$$E \equiv \beta E_p,$$

where E_p is the potential evaporation rate. The coefficient β is related to the soil moisture deficit and plant resistance to transpiration (Monteith, 1981). In the present discussion, interaction between these processes and potential evaporation are not considered. Instead β is arbitrarily varied in order to study the potential sensitivity of the modelled atmospheric boundary layer to the availability of surface moisture.

The computation of E_p follows the modified Penman method presented in Mahrt and Ek (1984) except for modification to increase numerical efficiency and explicit dependence of upward longwave radiation on temperature. The original Penman method requires knowledge of the net radiation and eliminates surface temperature as a parameter. Here, however, we need the surface temperature for radiation and surface heat flux calculations, and we therefore use (A1) to determine T_0 in the manner outlined below (A2-A3).

The usual Penman method is based on a linearization of the saturation vapour pressure in terms of the temperature difference between the lowest atmospheric level and the surface. Linearizing the upward radiation, we obtain

$$\sigma T_0^4 \simeq \sigma T_1^4 \left(1 + 4 \left(\frac{T_0 - T_1}{T_1} \right) \right). \quad (\text{A2})$$

Then use of the Penman approach leads to the following version for the potential evaporation:

$$E_p = [R\Delta + \rho L c_h u (q_1^* - q_1)] / (1 + \Delta + r) \quad (\text{A3})$$

with

c_h = exchange coefficient for heat,

ρ = density,

L = heat of evaporation for water,

c_p = specific heat of air at constant pressure,

$$r = \left(\frac{4\sigma R_{\text{gas}}}{c_p} \right) \frac{T_1^4}{p c_h u},$$

σ = Stefan-Boltzman constant,

p = surface pressure,

R_{gas} = gas constant assumed equal to dry-air value,

$$\Delta = \left(\frac{L^2 \varepsilon}{R_{\text{gas}} c_p} \right) q_1^* T_1^{-2},$$

ε = ratio of water molecular weight to that of dry air = 0.622,

q_1 = specific humidity at atmospheric level,

q_1^* = saturation specific humidity at temperature T_1 ,

T_1 = temperature at atmospheric level,

$R = ((1 - \alpha)S\downarrow + L\downarrow - \sigma T_1^4 - G)$.

The extra factor, r , which appears in (A3) but not in the usual Penman relationship, is due to estimation of the upward radiation in terms of the surface temperature.

Given $E = \beta E_p$, (A1) is then used to estimate T_0 .

As in previous models, we do not distinguish between the surface air temperature at the level of the roughness elements as used in surface-layer similarity theory and the effective surface radiation temperature. Without this assumption, we would need a more detailed formulation of surface conditions than is included in the present development. It should also be noted that model surface temperatures have an uncertain relationship to the actual temperature of the soil surface or plant canopy. The latter are difficult to define or measure in actual field situations.

Appendix B. Numerical Techniques

The time integration of the change of mean profiles due to boundary-layer turbulence reduces to the solution of the diffusion equation

$$\frac{\partial X}{\partial t} = \frac{\partial}{\partial z} K_x \left(\frac{\partial X}{\partial z} - \gamma \right), \quad (\text{B1})$$

where $X = [u, v, \theta, q]$. At each time step, the mean profiles are used first to calculate drag coefficients c_m and c_h from Louis (1979) and then to calculate the surface fluxes. Next,

boundary-layer height is estimated for computation using (10) with $\theta_s = \theta_0$, where θ_0 is the surface virtual temperature obtained from the surface energy balance (Appendix A). Under convective conditions (positive surface heat flux), Equation (11) is then used together with (12) and (10) to obtain an improved estimate for the boundary-layer height h . Equation (B1) is then used to step forward one time step using the diffusivity profile (1). The layer between the ground and the first atmospheric level is treated as an equilibrium surface layer and (B1) is employed only above this layer. The boundary conditions thus become flux conditions at the lowest model level. The boundary-layer height, h , the countergradient correction term, and the surface values of temperature, θ_0 , and humidity, q_0 , are assumed constant during each time step. In order to ensure computational stability with large time steps, it is necessary to use an implicit integration technique; here we use the fully implicit Cranck-Nicholson scheme (or Laasonen schema) given by

$$X^{(n+1)} - X^{(n)} = \Delta t \frac{\partial}{\partial z} K_x \frac{\partial}{\partial z} X^{(n+1)}, \quad (\text{B2})$$

Where the superscripts designate the time level. For the spatial operator, we employ a variation of the finite-element method using Chapeau functions for the mean variables. Some care must be taken to ensure that no unnecessary truncation errors are introduced. The model is intended to be used with only a few grid levels in the boundary layer. Therefore, the large variation of the diffusivities near the top of the boundary layer will typically not be adequately resolved. To minimize truncation errors from finite differencing of the diffusivity profile, we use the finite-element technique with the analytical form of K from (1). The method can be developed as follows: suppose X is written in terms of some expansion in basic functions $\alpha_k(z)$. Multiplying by $\alpha_k(z)$ on both sides of (B2) and integrating from the lowest level to the top of the boundary layer yields

$$A_{ki} \left(X_i^{(n+1)} - X_i^{(n)} \right) = B_{ki} X_i^{(n+1)} \quad (\text{B3})$$

with

$$A_{ki} = \int_{z_i}^{z_N} \alpha_k(z) \alpha_i(z) dz,$$

$$B_{ki} = \Delta t \int_{z_i}^{z_N} \alpha_k(z) \frac{\partial}{\partial z} K(z) \frac{\partial}{\partial z} \alpha_i(z) dz.$$

where summation occurs over repeated indices.

We use Chapeau functions for the basic functions defined on the grid as

$$\alpha_i(z) = \begin{cases} \frac{z - z_{i-1}}{z_i - z_{i-1}} & \text{for } z_{i-1} \leq z \leq z_i, \\ \frac{z_{i+1} - z}{z_{i+1} - z_i} & \text{for } z_i \leq z \leq z_{i+1}, \end{cases} \quad (\text{B4})$$

and zero outside the interval $z_{i-1} - z_{i+1}$. These functions span all piecewise linear functions on the grid. Using (B4) and (1), A_{ki} and B_{ki} are easily computed. Solution of the diffusion step then becomes

$$(A_{ki} - B_{ki})X_i^{n+1} = A_{ki}X_i^n. \quad (\text{B5})$$

The expansion coefficients X_i are simply the gridpoint values by virtue of our choice for α_i in (B4).

We find by integration

$$\begin{aligned} A_{ii+1} &= \Delta z_i / 6, & (\Delta z_i &\equiv z_{i+1} - z_i). \\ A_{ii-1} &= \Delta z_{i-1} / 6, & A_{ii} &= \frac{1}{3}(\Delta z_{i-1} + \Delta z_i), \end{aligned} \quad (\text{B6})$$

All other terms are zero.

For B_{ki} we find that

$$\begin{aligned} B_{ii-1} &= \frac{\Delta t}{\Delta z_{i-1}^2} \int_{z_{i-1}}^{z_i} K(z) dz, \\ B_{ii+1} &= \frac{\Delta t}{\Delta z_i^2} \int_{z_i}^{z_{i+1}} K(z) dz, \\ B_{ii} &= -(B_{ii-1} + B_{ii+1}). \end{aligned} \quad (\text{B7})$$

The integrals of K over one grid interval are found to be sufficiently accurate when approximated by the center value multiplied by Δz , except for the integral over the interval containing the top of the boundary layer, where we instead use the approximation

$$\int_{z_k}^{z_{k+1}} K(z) dz = \int_{z_k}^h K(z) dz = (h - z_k) K\left(\frac{h + z_k}{2}\right). \quad (\text{B8})$$

References

- André, J. C., De Moor, G., Lacerrère, P., Therry, G., and Vachat, R.: 1978, 'Modelling the 24 Hour Evolution of the Mean and Turbulent Structures of the Planetary Boundary Layer', *J. Atmos. Sci.* **35**, 1861-1883.
- André, J. C. and Mahrt, L.: 1982, 'The Nocturnal Surface Inversion and Influence of Clear-Air Radiative Cooling', *J. Atmos. Sci.* **39**, 864-878.
- Anthes, R. A., Kuo, Y.-H., Benjamin, S. G., and Li, Y.-F.: 1982, 'The Evolution of the Mesoscale Environment of Severe Local Storms: Preliminary Modeling Results', *J. Cli. Appl. Meteorol.* **9**, 1187-1213.
- Binkowski, F. S.: 1983, 'A Simple Model for the Diurnal Variation of the Mixing Depth and Transport Flow', *Boundary-Layer Meteorol.* **27**, 217-236.
- Brost, R. A. and Wyngaard, J. C.: 1978, 'A Model Study of the Stably Stratified Boundary Layer', *J. Atmos. Sci.* **8**, 1427-1440.
- Busch, N. E., Chang, S. W., and Anthes, R. A.: 1976, 'A Multi-Level Model of the Planetary Boundary Layer Suitable for Use with Mesoscale Dynamical Models', *J. Appl. Meteorol.* **15**, 909-919.
- Businger, J. A., Wyngaard, J. C., Izumi, Y., and Bradley, E. F.: 1971, 'Flux-Profile Relationships in the Atmospheric Surface Layer', *J. Atmos. Sci.* **28**, 181-189.
- Chang, S. W.: 1979, 'An Efficient Parameterization of Convective and Nonconvective Planetary Boundary Layers for Use in Numerical Models', *J. Appl. Meteorol.* **18**, 1205-1215.

- Chang, S. W.: 1981, 'Test of a Planetary Boundary Layer Parameterization Based on a Generalized Similarity Theory in Tropical Cyclone Models', *Mon. Wea. Rev.* **109**, 843–853.
- Clarke, R. H.: 1970, 'Recommended Methods for the Treatment of the Boundary Layer in Numerical Models of the Atmosphere', *Austr. Meteorol. Mag.* **18**, 51–73.
- Clarke, R. H., Dyer, A. J., Brook, R. R., Reid, D. C., and Troup, A. J.: 1971, 'The Wangara Experiment: Boundary Layer Data', Tech. Paper No. 19, Div. Met. Phys., CSIRO, Australia.
- Deardorff, J. W.: 1966, 'The Counter Gradient Heat Flux in the Lower Atmosphere and in the Laboratory', *J. Atmos. Sci.* **23**, 503–506.
- Deardorff, J. W.: 1972, 'Parameterization of the Planetary Boundary Layer for Use in General Circulation Models', *Mon. Wea. Rev.* **100**, 93–106.
- Deardorff, J. W.: 1973, 'The Use of Subgrid Transport Equations in a Three-Dimensional Model of Atmospheric Turbulence', *J. Fluids Engr.* **95**, 429–438.
- Deardorff, J. W.: 1974, 'Three-Dimensional Study of the Height and Mean Structure of the Planetary Boundary Layer', *Boundary-Layer Meteorol.* **15**, 1241–1251.
- Højstrup, J.: 1982, 'Velocity Spectra in the Unstable Planetary Boundary Layer', *J. Atmos. Sci.* **39**, 2239–2248.
- Holton, J. R., Wallace, J. M., and Joung, J. A.: 1971, 'On Boundary Layer Dynamics and the ITCZ', *J. Atmos. Sci.* **28**, 275–280.
- Holtstag, A. A. M. and Van Ulden, A. P.: 1983, 'A Simple Scheme for Daytime Estimates of Surface Fluxes from Routine Weather Data', *J. Cli. Appl. Meteorol.* **22**, 517–529.
- Holzworth, G. C.: 1964, 'Estimates of Mean Maximum Mixing Depths in the Contiguous United States', *Mon. Wea. Rev.* **92**, 235–242.
- Louis, J.-F.: 1979, 'A Parametric Model of Vertical Eddy Fluxes in the Atmosphere', *Boundary-Layer Meteorol.* **17**, 187–202.
- Mahrt, L.: 1981, 'Modelling the Depth of the Stable Boundary Layer', *Boundary-Layer Meteorol.* **21**, 3–19.
- Mahrt, L. and Ek, M.: 1984, 'The Influence of Atmospheric Stability on Potential Evaporation', *J. Cli. Appl. Meteorol.* **23**, 222–234.
- Mahrt, L., Heald, R. C., Lenschow, D. H., Stankov, B. B., and Troen, I.: 1979, 'An Observational Study of the Structure of the Nocturnal Boundary Layer', *Boundary-Layer Meteorol.* **17**, 247–264.
- Mailhôt, J., and Benoit, R.: 1982, 'A Finite-Element Model of the Atmospheric Boundary Layer Suitable for Use with Numerical Weather Prediction Models', *J. Atmos. Sci.* **39**, 2249–2266.
- Manins, P. C.: 1982, 'The Daytime Planetary Boundary Layer: A New Interpretation of Wangara Data', *Quart. J. R. Meteorol. Soc.* **108**, 689–705.
- McCumber, M. C. and Pielke, R. A.: 1981, 'Simulation of the Effects of Surface Fluxes of Heat and Moisture in a Mesoscale Numerical Model Soil Layer', *J. Geophys. Res.* **86**, 9929–9938.
- Monteith, J. L.: 1981, 'Presidential Address: Evaporation and Surface Temperature', *Quart. J. R. Meteorol. Soc.* **107**, 1–24.
- Pan, H.-L. and Mahrt, L.: 1986, 'Interaction Between Soil Hydrology and Boundary-Layer Development', *Boundary-Layer Meteorol.*, submitted.
- Pielke, R. A. and Mahrer, Y.: 1975, 'Technique to Represent the Heated Boundary Layer in Mesoscale Models with Coarse Vertical Resolution', *J. Atmos. Sci.* **32**, 2288–2309.
- Priestley, C. H. B. and Swinbank, W. C.: 1947, 'Vertical Transport of Heat by Turbulence in the Atmosphere', *Proc. R. Soc.* **A189**, 543–561.
- Smeda, M. S.: 1979, 'A Bulk Model for the Atmospheric Planetary Boundary Layer', *Boundary-Layer Meteorol.* **14**, 411–428.
- Tennekes, H.: 1973, 'A Model for the Dynamics of the Inversion above a Convective Boundary Layer', *J. Atmos. Sci.* **30**, 558–567.
- Therry, G. and Lacarrère, P.: 1983, 'Improving the eddy kinetic energy model for planetary boundary layer description', *Boundary-Layer Meteorol.* **25**, 63–88.
- Wyngaard, J. C. and Brost, R. A.: 1984, 'Top-Down and Bottom-Up Diffusion in the Convective Boundary Layer', *J. Atmos. Sci.* **41**, 102–112.
- Yamada, T. and Mellor, G.: 1975, 'A Simulation of the Wangara Atmospheric Boundary Layer Data', *J. Atmos. Sci.* **32**, 2309–2329.
- Yu, T.-W.: 1977, 'A Comparative Study on Parameterization of Vertical Turbulent Exchange Processes', *Mon. Wea. Rev.* **105**, 57–66.
- Zhang, D. and Anthes, R. A.: 1982, 'A High-Resolution Model of the Planetary Boundary Layer – Sensitivity Tests and Comparisons with SESAME-70 Data', *J. Appl. Meteorol.*, 1594–1609.